Journal of Coastal Research	17	2	468–481	West Palm Beach, Florida	Spring 2001

Flow Kinematics of Low-energy Rip Current Systems

Robert W. Brander† and Andrew D. Short‡

†School of Geography
University of New South Wales
Sydney, NSW 2052, Australia

‡Coastal Studies Unit
School of Geosciences
University of Sydney
Sydney, NSW 2006, Australia

ABSTRACT

BRANDER, R.W. and SHORT, A.D., 2001. Flow Kinematics of Low-energy Rip Current Systems, *Journal of Coastal Research,* 17(2), 468–481. West Palm Beach (Florida), ISSN 0749-0208.

Measurements of hydrodynamics and topography were obtained during two separate field experiments at Palm Beach, NSW, Australia in order to assess flow characteristics within rip current systems during accretionary conditions. At an evolutionary time scale (days–weeks), feeder channel flow decreased and rip-neck flow velocity increased during a cycle of intermediate beach state evolution. At shorter time scales (hours), rip current velocity is inversely related to changes in water depth and is clearly modulated by the tide. Spatially, rip current velocity increases progressively both longshore from the feeders to the rip-neck and offshore within the rip-neck itself. Flow velocity is not constant across the rip channel and increases towards the middle and deeper section of the rip channel. Vertical velocity profiles within the rip-neck and feeder channels show an initial increase in flow magnitude above the bed, with maxima towards the middle of the flow and then a subsequent decrease towards the surface. Evidence of pulsatory rip flow behaviour was found at infragravity frequencies in both rip-feeder and rip-neck environments. Infragravity energy was dominant in the feeder channels during the observed beach state evolution and increased in the rip-neck as the system evolved towards transverse bar and low tide terrace and rip beach states. There is evidence to suggest that topography may exert direct controls on rip flow. The results of this study provide both new quantitative information on the flow kinematics of rip currents and confirm findings of previous studies.

ADDITIONAL INDEX WORDS: *Rip currents, intermediate beaches, coastal morphodynamics, infragravity energy.*

INTRODUCTION

Rip currents are common features on many of the world's sandy beaches and their overall significance to nearshore circulation, offshore sediment transport, pollution dispersal, and recreational swimmers has long been recognised by scientists and the general public alike (*e.g.* SHEPARD *et al.* 1941; MCKENZIE, 1958; BASCO, 1983; SHORT, 1985; SHORT and HOGAN, 1994). It is therefore of some concern that due to a paucity of appropriate field data, our present knowledge of the kinematics and dynamics of flow in rip current systems remains limited. Although several field studies have measured rip current velocities directly (*e.g.* SHEPARD and INMAN, 1950; SONU, 1972; SASAKI and HORIKAWA, 1975; TALBOT and BATE, 1987a,b; BOWMAN *et al.,* 1988a; 1988b; 1992; HUNTLEY *et al.,* 1988; SMITH and LARGIER, 1995; AAGAARD *et al.,* 1997; BRANDER, 1999), these have either been restricted largely to measurements of surface flows, or have been limited by spatial and temporal logistical constraints. In particular, no study has assessed the variations in characteristic flow behaviour during commonly occurring sequences of beach-state change under either increasing or decreasing wave energy conditions.

Rip flow is often associated with the existence of both rip feeder and rip-neck components, which carry flow in the alongshore and offshore directions respectively (KOMAR, 1998). On intermediate beaches with pronounced surf zone morphology, these components are contained within distinct channels and their variation in morphological expression is well-described by the morphodynamic beach stage model of WRIGHT and SHORT (1984). Where such pronounced rip topography exists, rip flow has traditionally been thought to be maintained through the alongshore variation in pressure gradients formed as a result of wave energy dissipation and wave set-up being larger across the barred areas between rip channels (*e.g.* SONU, 1972; WRIGHT *et al.,* 1979; AAGAARD and MASSELINK, 1999). The velocity of rip flow has therefore been assumed to be primarily controlled by fluctuations in the amount of water carried across the bars and the magnitude of the pressure gradients driving water into the rip. With the exception of studies by SONU (1972), FOX and DAVIS (1974), and BRANDER (1999), little attention has focussed directly on the role of topographic control on rip current flow. This is hardly surprising, given the difficulty involved in obtaining detailed topographic information in such a logistically demanding environment.

The purpose of this study is to describe and quantify the kinematic behaviour of rip current systems based on measurements obtained during two separate field experiments. The first encompassed an almost complete low-energy beach state evolution (WRIGHT and SHORT, 1984) from longshore bar and trough morphology (LBT) through to incipient low-tide terrace and rip morphology (LTT). The second involved concurrent measurements from three adjacent low-energy transverse bar and rip (TBR) systems. It should be noted that no globally adopted definition distinguishing between "low"

98018 received 19 February 1998; accepted in revision 10 October 2000.

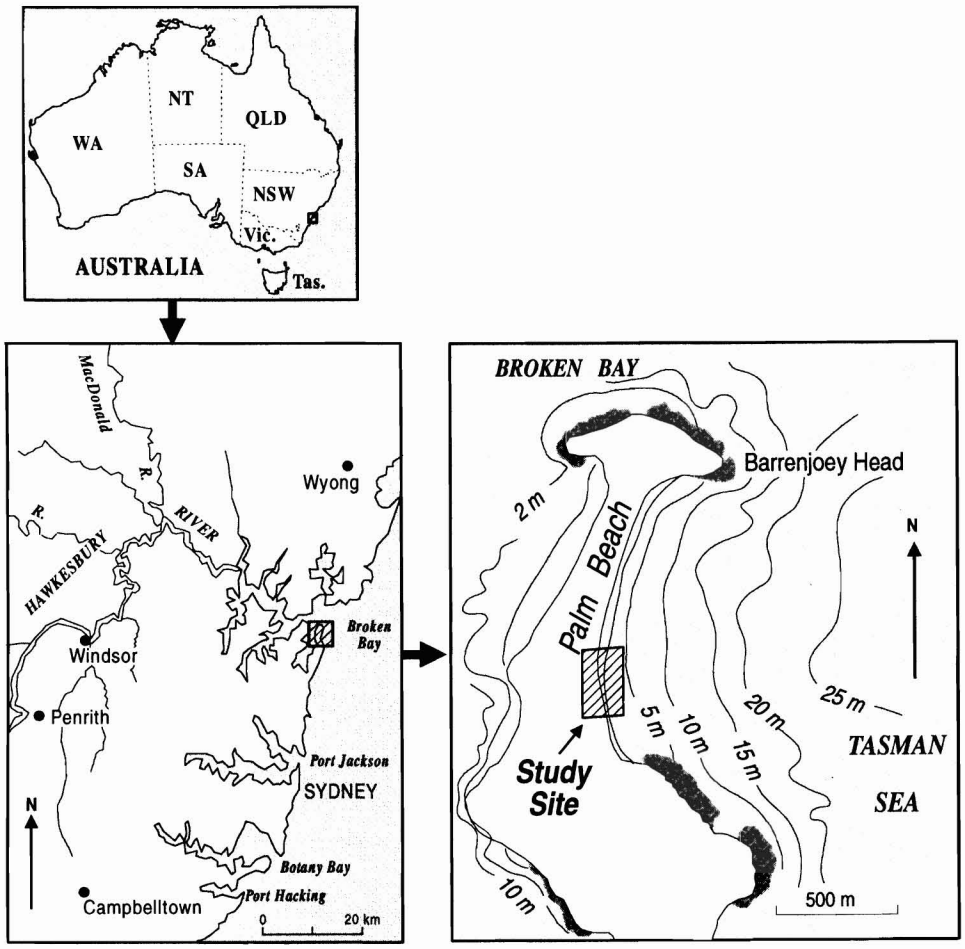

Figure 1. Maps of the location of Palm Beach, NSW, Australia, showing the study site at the southern end of the beach.

and "high" energy conditions presently exists within the literature, but in this study "low-energy" is used to describe decreasing, or stable, energy conditions when breaking wave heights are less than 1 m.

Specifically, the aims of this study are to examine: i) the behaviour of rip-neck and feeder current flow at both evolutionary (days) and instantaneous (hours-minutes) time scales; ii) spatial gradients in rip flow; and iii) basic characteristics of both rip-neck and feeder channel flow. In particular, the potential influence of channel morphology on rip flow will be examined.

STUDY SITE

The field experiments were conducted at Palm Beach, New South Wales, Australia (Figure 1) from 18–24 April, 1994 (PB1) and 18–20 June, 1994 (PB2). Palm Beach is a 2.3 km long sandy, intermediate beach, facing north-east and bounded by headlands. The site experiences a highly variable wind-wave climate superimposed on persistent moderate- to-high energy south-easterly swell with modal wave height and wave periods of 1.6 m and 10 s respectively (SHORT and TRENAMAN, 1992). Tides are semi-diurnal with mean spring tide ranges of 1.6 m (WRIGHT *et al.*, 1980). The beach is moderately sloping (S = 0.023) and inshore sediments are composed primarily of well-rounded and sorted quartz sands with median grain diameters less than 0.35 mm.

METHODS

The nearshore morphology was surveyed daily using a theodolite and stadia rod at low tide along nine (PB1) and seven (PB2) cross-shore transects established at 25 m intervals along the beach centred around a primary zero-transect. Water surface elevations and longshore and cross-shore current velocities were measured respectively using 5 strain gauge pressure sensors and 9 bi-directional, ducted impellor flow meters. The sensors were mounted in various combinations on weighted, portable pods designed for use in the surf zone. Hydrodynamic stations were referred to as Pods 1 through 5 (P1–P5). A summary of daily instrument pod locations relative to components of the rip system is shown in Figures 2 and 3 and the sensor combinations and elevations are provided in Table 1. Additional qualitative information on near-

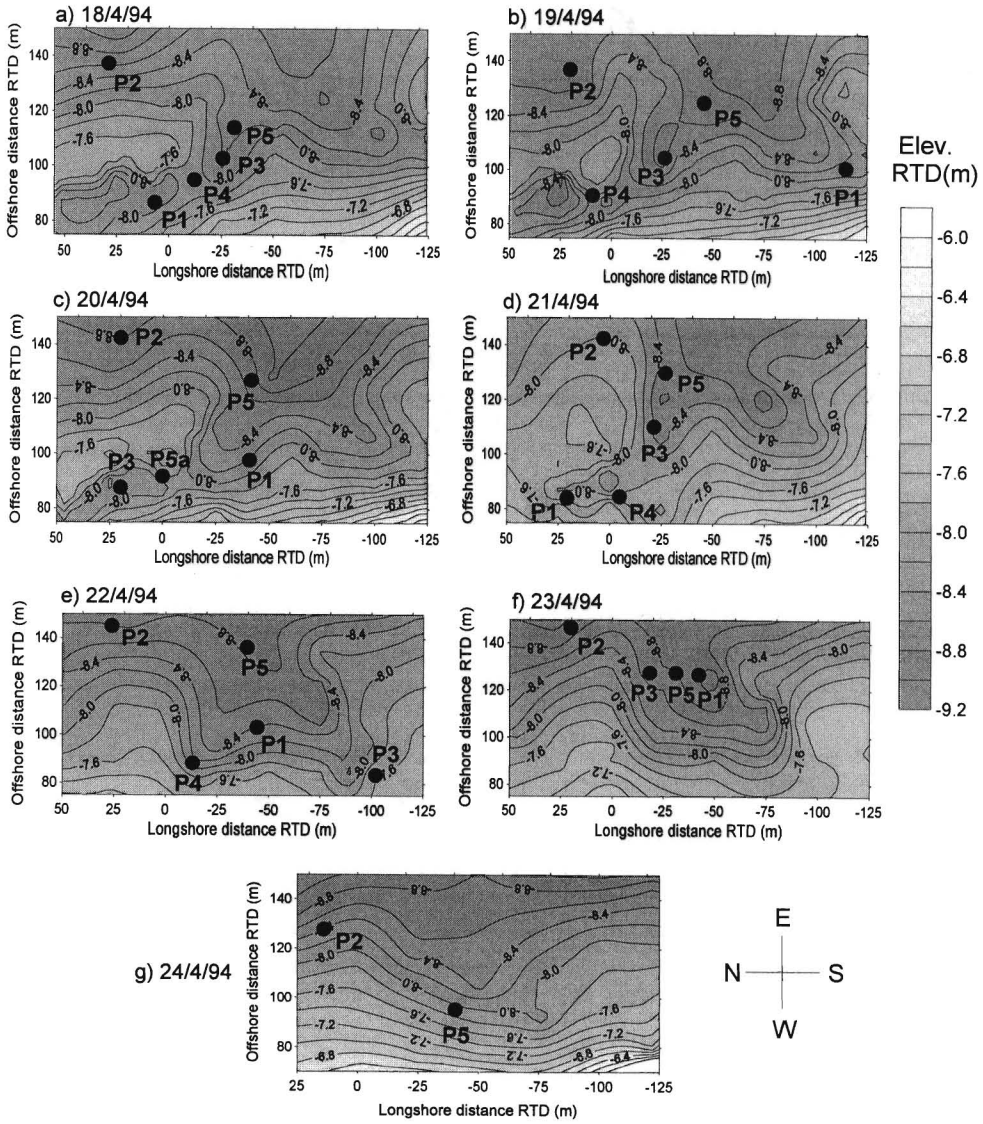

Figure 2. Contour plots of rip system configuration during the Palm Beach 1 (PB1) experiment showing instrument pod locations (P1, P2. . .P5) on: a) 18/4/94; b) 19/4/94; c) 20/4/94 (P5 was moved to P5a towards end of experiment); d) 21/4/94; e) 22/4/94; f) 23/4/94; and g) 24/4/94. RTD = relative to survey datum.

shore circulation patterns was obtained from multiple releases of potassium permanganate dye.

The pods were deployed as close to low tide as possible and the flow meters were oriented along the dominant axis of flow in both the feeder and rip-neck channels. This orientation was ascertained by dye release and in-situ observations and is considered accurate for the time of deployment. Nevertheless, it must be acknowledged that due to logistical constraints, the flow meter orientations remained fixed during each daily deployment and therefore may not have recorded maximum flows if the location of this region shifted. However, trajectory patterns of dye releases made at regular intervals each day indicated that flow concentration remained relatively stable during the deployments, consistently passing over the locations of the pods.

All sensors were hardwired to a shore-based mobile laboratory, where the data was collected at a sampling frequency of 2 Hz for 34 minutes with runs separated by varying intervals. Data collection periods were dependant on the timing of the daily low tide and varied from 4–8 hours each day during the experiments. Measurements of offshore significant wave height (H_o) and peak wave period (T_p) were obtained from a waverider buoy (NSW PUBLIC WORKS, 1994) located approximately 4 km offshore and 14 km south of Palm Beach. Readings from the pressure sensors were converted to water-surface elevation using NIELSEN'S (1988) method of local ap-

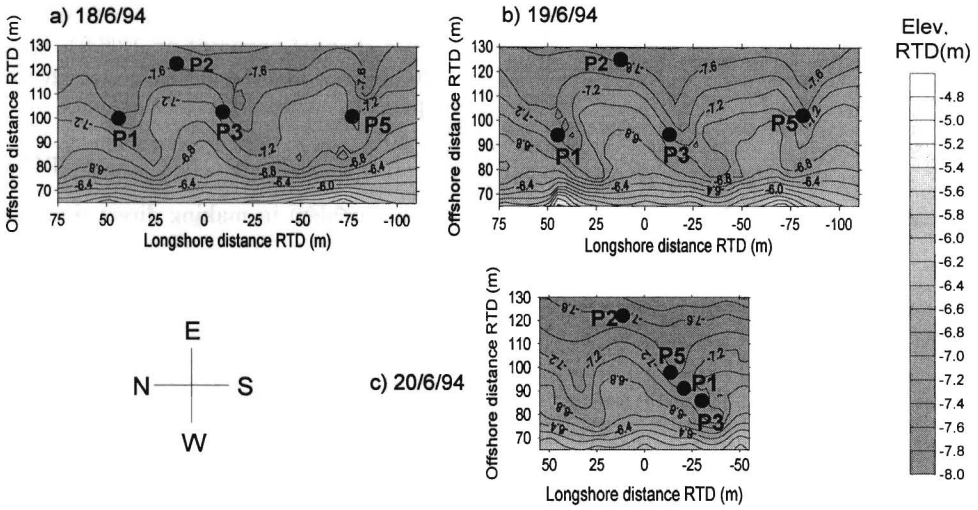

Figure 3. Contour plots of rip system configuration during the Palm Beach 2 (PB2) experiment showing instrument pod locations (P1, P2, P3, P5) on: a) 18/6/94; b) 19/6/94; and c) 20/6/94. RTD = relative to survey datum.

proximations. Flow-meter data were corrected for frequency-response characteristics using the techniques of NIELSEN and COWELL (1981). Estimates of root-mean-square wave height (H_{rms}) were obtained using the standard deviation (σ) of the pressure sensor records: $H_{rms} = 2.8\sigma$ (CERC, 1984).

Auto-spectral analysis was used to determine the amount of variance associated with incident wind wave frequencies of 0.5–0.125 Hz (2–8 s), incident swell waves frequencies of 0.125–0.05 Hz (8–20 s) and infragravity frequencies of 0.05–0.0005 Hz (20–2000 s) (HEGGE and MASSELINK, 1996; AAGAARD and MASSELINK, 1999). The total amount of variance at these broad wind, swell, and infragravity frequency bands are referred to as σ^2_w, σ^2_s, and σ^2_{inf}. Using the total amount of variance contained in the time series σ^2_{tot}, the proportion of infragravity energy, *%inf* is computed according to: $\%inf = 100(\sigma^2_{inf}/\sigma^2_{tot})$. The proportion of wind and swell energy, *%wind* and *%swell,* is similarly computed by using σ^2_w and σ^2_s.

Table 1. *Summary of instrument heights above the bed for the pods deployed during both experiments. All values are in units of m's.* ND = *not deployed; p = pressure; u = cross-shore flow; and v = longshore flow. As noted in text, u and v were aligned along the dominant axis of current flow when deployed in the rip-neck and feeder channels respectively. See Figure 2 and Figure 3 for pod locations.*

Day	Pod 1 (P1)	Pod 2 (P2)	Pod 3 (P3)	Pod 4 (P4)	Pod 5 (P5)
18/4/94	p = 0.10 u = 0.40 v = 0.40	p = 0.10	p = 0.10 u = 0.40 v = 0.40	p = *0.10* v = 0.40	p = 0.10 u = 1.00, 0.60
19/4/94	p = 0.10 u = 0.40 v = 0.40	p = 0.10	p = 0.10 u = 0.40 v = 0.40	p = *0.10* v = 0.40	p = 0.10 u = 1.00, 0.70, 0.40
20/4/94	p = 0.10 u = 0.40 v = 0.40	p = 0.10	p = 0.10 u = 0.40 v = 0.40	*ND*	p = 0.10 u = 1.00, 0.80, 0.30
21/4/94	p = 0.10 u = 0.40 v = 0.40	p = 0.10	p = 0.10 u = 0.40 v = 0.40	p = *0.10* v = 0.40	p = 0.10 u = 1.00, 0.80, 0.30
22/4/94	p = 0.10 u = 0.40 v = 0.40	p = 0.10	p = 0.10 v = 0.40	p = *0.10* v = 0.40	p = 0.10 u = 1.00, 0.70, 0.30
23/4/94	p = 0.10 u = 0.70, 0.30	p = 0.10	p = 0.10 u = 0.70, 0.30	*ND*	p = 0.10 u = 1.00, 0.70, 0.30
24/4/94	*ND*	p = 0.10	*ND*	*ND*	p = 0.10 u = 0.60, 0.30
18/6/94	p = 0.10 u = 0.70, 0.30	p = 0.10	p = 0.10 u = 0.70, 0.30	*ND*	p = 0.10 u = 0.70, 0.50, 0.30
19/6/94	p = 0.10 u = 0.70, 0.30	p = 0.10	p = 0.10 u = 0.70, 0.30	*ND*	p = 0.10 u = 1.00, 0.70, 0.50, 0.30
20/6/94	p = 0.10 u = 0.70, 0.30	p = 0.10	p = 0.10 u = 0.30	*ND*	p = 0.10 u = 1.00, 0.50, 0.30

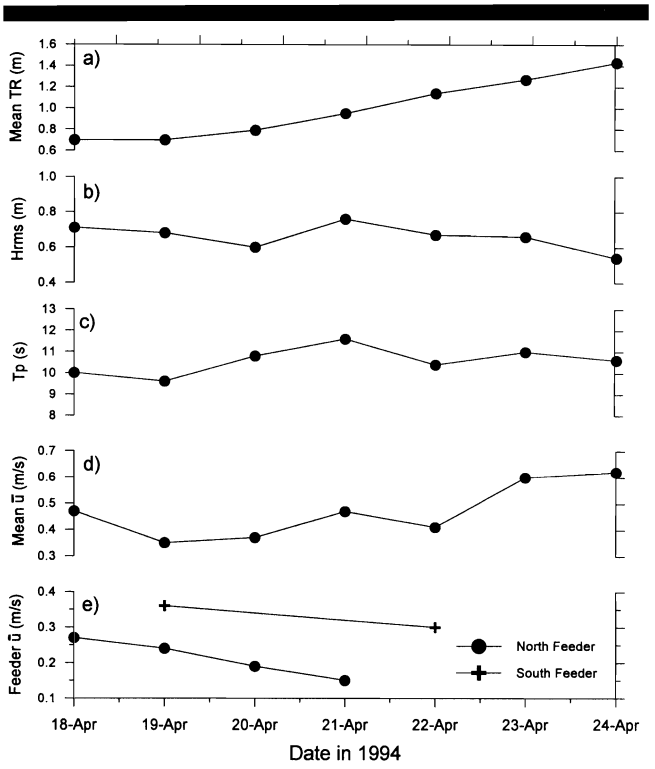

Figure 4. Summary of hydrodynamic parameters and flow velocity measurements between 18/4–24/4/94 (PB1) showing daily variations in: a) Tide range (*TR*); b) Mean H_{rms}; c) Mean T_p ; d) Mean rip-neck flow velocity ($\bar{u}_r$); and e) Mean flow velocity ($\bar{u}$) in the north and south feeders.

ENVIRONMENTAL SUMMARY

The first experiment encompassed most of a neap-spring tidal cycle with mean neap tide ranges of 0.7 m on 18/4/94 increasing to 1.4 m at the onset of the spring tides on 24/4/1994 (Figure 4a). Swell waves from the south-east were present throughout the experiment with H_{rms} decreasing from 0.71 m to 0.54 m over the same period (Figure 4b) while T_p varied from 8–12 s (Figure 4c). The measurement period is indicative of decreasing energy conditions following a storm event which occurred on 14/4/1994 having offshore wave heights in excess of 4 m. Changes in the morphological configuration of the rip system over the 7 day period are illustrated in the contour plots in Figure 2. On 18/4/94 the nearshore system exhibited longshore bar and rip morphology with two distinct feeder channels (Figure 2a). Over time, the bars migrated landward infilling the feeder channels and causing a constriction of the main rip channel. The southern feeder became the dominant feeder channel and completely merged into the main rip channel when the system evolved into transverse bar and rip morphology on 23/4/94 (Figure 2f). At the end of the experiment, the system exhibited incipient low-tide terrace morphology (Figure 2g).

The second experiment coincided with low energy swell waves from the south-east (H_{rms} = 0.4–0.5 m; T_p = 8–10 s) and a small increase in tide range from 1.0 to 1.2 m. The beach exhibited well-developed transverse bar and rip morphology with three closely spaced rip currents situated within the study area (Figure 3). Aside from infilling of the smaller feeder channel apparent on 18/6/94, the morphological configuration of the system did not change dramatically over the experiment (Figure 3).

TEMPORAL RIP FLOW BEHAVIOUR

One problem in making direct comparisons of rip system flow velocity between various stages of the morphologic evolution observed during PB1 is that the instrument pods were placed in different locations each day and were fixed in location during each deployment (Figures 2 and 3). Although the pods were initially deployed in the region of fastest flow, it is impossible to state with 100% confidence that each day of measurement was in fact recording maximum flows in the rip-neck and feeder channels at all times. In fact, this is highly improbable. However, as mentioned previously, dye release and direct observations support the trends in Figure 4d,e which show that the dominant characteristic of current flow patterns during PB1 was an overall increase in velocity in the rip-neck and a steady reduction in flow velocity in the northern feeder. It should be noted that in order to reduce temporal and tidal bias between days, the flow measurements summarised in Figure 4d,e were recorded over similar tidal stages. In general, mean rip-neck flow velocity ($\bar{u}_r$) increased from a range of approximately 0.35–0.45 m s^{-1} from 18/4–21/4/94 to approximately 0.6 m s^{-1} from 23/4–24/4/94 (Figure 4d). The northern feeder decreased in mean velocity from 0.27 m s^{-1} on 18/4/94 to 0.15 m s^{-1} on 21/4/94 (Figure 4e). The southern feeder, although measured on only two days, was the stronger of the two feeders, with mean velocities of approximately 0.3 m s^{-1}, and did not change significantly over time (Figure 4e).

Tidal modulation of rip velocity remained a factor throughout each stage of morphological evolution during PB1 with $\bar{u}_r$ increasing towards low tide and decreasing towards high tide during both LBT and TBR conditions (Figure 5a,b). Feeder flow was similarly affected, attaining maxima at low tide and subsequently decreasing with increasing water depth (Figure 5c). During PB2, flow in all three rips decreased so rapidly during the rising tide that rip flow may have ceased entirely at high tide (Figure 5d).

In order to examine the effect of changing depth on rip velocity in greater detail, the mean depth ($\bar{h}$) was related to $\bar{u}_r$ recorded at the middle sensor ($z \cong 0.7$ m) for PB1. This sensor elevation was chosen for comparison since measurements at this elevation were available for every data run over the course of the experiment. To account for changing hydrodynamic and energy conditions between days, $\bar{u}_r$ was non-dimensionalised by H_{rms}/T_p and to account for changing tidal levels, $\bar{h}$ was non-dimensionalised by the local water depth at high tide (h_{ht}). As illustrated in Figure 6, flow velocity in the rip-neck is strongly influenced by water depth as shown by an exponential function (R^2 = 0.76) of the form

$$\bar{u}/(H_{rms}T) = 25.6\exp[-1.9(\bar{h}/h_{HT}) \quad (1)$$

suggesting that rip-neck velocity decreases with increasing water depth. Although other statistical functions provided a

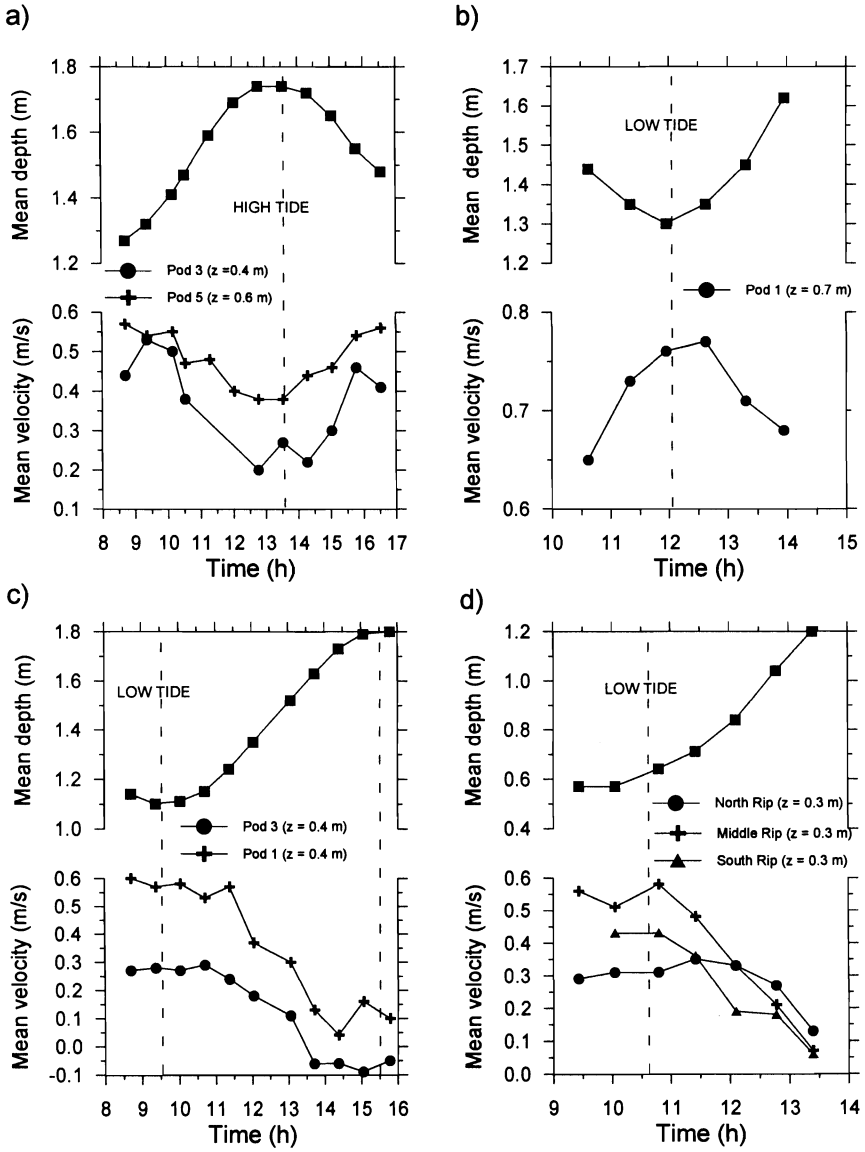

Figure 5. Tidal modulation of rip system velocity as illustrated by fluctuations in mean water depth ($\bar{h}$) and mean flow velocity ($\bar{u}$) in: a) the rip-neck on 18/4/94; b) the rip-neck on 23/4/94; c) the northern feeder on 20/4/94; and d) all three rip-necks on 19/6/94.

better fit to the data, the exponential relationship was chosen since velocity and frictional resistance under waves and currents are known to decrease exponentially away from the bottom bed (NIELSEN, 1992).

SPATIAL RIP FLOW BEHAVIOUR

During the period of extended LBT conditions from 18/4 to 21/4/94 (Figure 2a–d), flow in the rip system progressively increased in velocity from the feeders seaward to the rip-neck (Figure 7a). This is particularly evident on 18/4 and 21/4/94 with mean flows in the north feeder increasing from 0.27 m s^{-1} and 0.15 m s^{-1} respectively to 0.47 m s^{-1} in the rip-neck (Figure 4d,e). This seaward increase in flow velocity is also evident from measurements made in the rip-neck of the middle rip during PB2 on 20/6/94. The trend line in Figure 7b represents an offshore increase in $\bar{u}_r$ from 0.24 to 0.36 to 0.41 m s^{-1}. Rip current velocity is also not constant across the rip channel, but increases towards the middle of the rip. Three pods were extended longshore across the rip channel on 23/4/94. The initial pod (P3) was situated approximately 15 m from the northern channel bank, whereas the last pod (P1) was located close to the channel thalweg (Figure 2f). The trend line in Figure 7c reflects a progressive increase in $\bar{u}_r$ of 0.54 to 0.60 m s^{-1} to 0.67 m s^{-1} from north to south. The vertical structure of rip system flow was examined using vertical arrays of three current meters (Table 1). Figure 8a illustrates that the recorded velocity in the rip-neck generally increases upwards in the flow, but is often characterised by

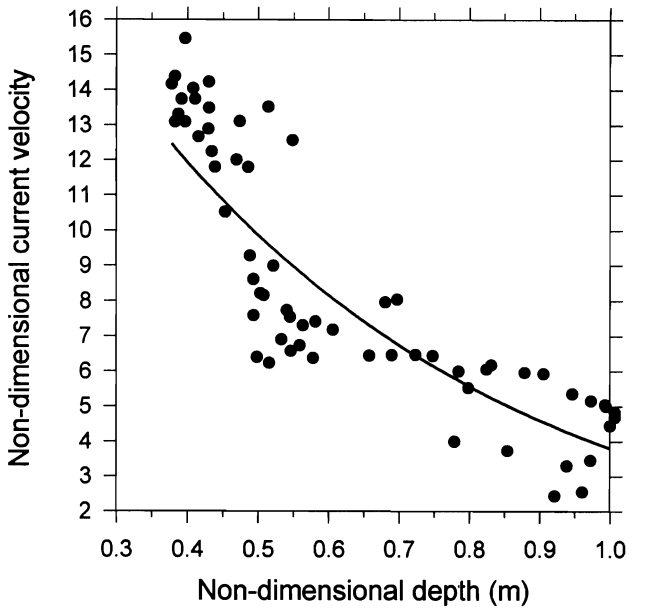

Figure 6. Relationship between non-dimensional rip-neck velocity ($\bar{u}_r/(H_{rms}/T_p)$) and non-dimensional water depth ($\hbar/\hbar_{ht}$). The exponential function shown is of the form: $\bar{u}/(H_{rms}T) = 25.6\exp[-1.9(\hbar/h_{HT})]$ ($R^2 = 0.76$).

a decrease in velocity close to the surface. This is also apparent in Figure 8b, which shows vertical velocity profiles made in the northern feeder when mean flows were relatively weak. Maximum velocities appear to occur at a relative depth (z/h) of approximately 0.5–0.75 in the rip-neck and 0.4–0.6 in the feeder.

RIP SYSTEM FLOW AND INFRAGRAVITY ENERGY

Temporal changes in rip-neck flow over the observed morphological evolution were examined in greater detail by comparing measurements made during LBT (19/4/94) and TBR (23/4/94) conditions at low tide. Raw and low-pass filtered (cut-off 0.01 Hz) time series of rip-neck current velocity shown in Figure 9 clearly illustrate that flow in the rip-neck (P5) was almost continuously offshore. Although the instantaneous velocity records show short periods of onshore flow corresponding to the passage of individual wave crests, these are simply minor velocity fluctuations superimposed on dominant offshore flow. These findings were typical of all the measurements obtained in the rip-neck. There are three major differences between the two data records. First, there is an increase in $\bar{u}_r$ from 0.52 to 0.77 m s^{-1}. Second is a corresponding increase in maximum instantaneous velocity (u_{max}) from approximately 1.5 to 2.0 m s^{-1}. Third, and perhaps most significant, is the evidence of current pulsing from the low pass filtered time series (Figure 9b). To examine the frequency band at which this pulsing occurs, variance density spectra were computed for both time series (Figure 9c). Both data records indicate significant amounts of energy at infragravity frequencies less than 0.025 Hz (40 s). On 19/4/94, this energy is distinctly "red" (AAGAARD and GREENWOOD, 1995), but on

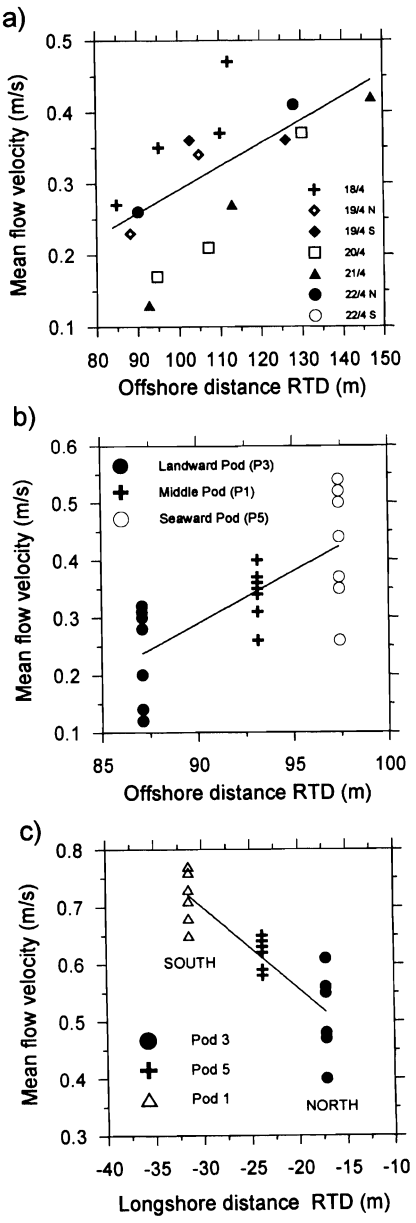

Figure 7. Spatial variation in rip system velocity as illustrated by: a) offshore increases in $\bar{u}$ from the feeders to the rip-neck for PB1; b) offshore increases in $\bar{u}$ in the rip-neck on 20/6/94; and c) cross-channel gradients in $\bar{u}$ in the rip-neck on 23/4/94. Lines of linear least squares regression are used only to illustrate general trends. RTD = relative to survey datum.

23/4/94 a strong peak at 0.0078 Hz (128 s) dominates the variance energy spectra (Figure 9c). It is also apparent from Figure 9c that the amount of energy associated with swell wave frequencies ($\cong$ 0.06–0.11 Hz) decreased over time, whereas the amount of infragravity energy had increased on 23/4/94. These pulses, which lasted for several minutes, were regular in occurrence and resulted in fluctuations of approximately $\pm$ 0.2–0.4 m s^{-1} about the mean rip-neck velocity (Figure 9b). This indicates that the flow velocity within the

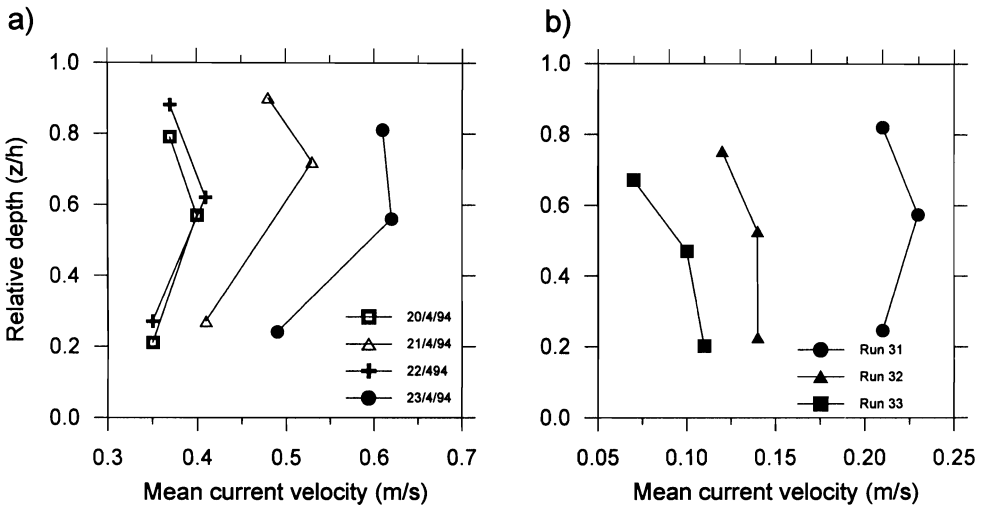

Figure 8. Vertical profiles of $\bar{u}$ in: a) the rip-neck during PB1; and b) three data runs in the northern feeder on 20/4/94. z/h = relative depth where z = sensor elevation.

rip-neck can increase (or decrease) by as much as 0.4–0.8 m s^{-1} in a very short period of time (seconds).

Time series of measured and low-pass filtered (cut-off = 0.01 Hz) flow velocities in the northern feeder (P1) near low tide are shown in Figure 10. The two data records represent end-points of the feeder evolution, since feeder channel morphology was well-established on 18/4/94, but had begun to narrow and infill by 21/4/94 (Figure 2). In the case of the former, flow in the feeder channel is similar to the rip-neck, in that it exists as an almost uninterrupted longshore unidirectional drift. This is evident from the flow record for 18/4/94 in Figure 10a, which shows an almost complete absence of northerly flows. By 21/4/94, the dominance of unidirectional flow in the northern feeder had clearly declined and it was observed through dye release that flow in the feeder at this time was greatly influenced by refracted and breaking waves propagating through the rip channel. Interestingly, although $\bar{u}$ decreased from 0.41 m s^{-1} to 0.27 m s^{-1} from 18/4 to 21/4/94 (Figure 10a), values of u_{max} were higher on 21/4/94 (approximately 1.2 m s^{-1} compared to 0.9 m s^{-1}). As was observed in the rip-neck, a significant amount of infragravity energy is present in the velocity spectra of the feeders for both days (Figure 10c). Both current spectra in Figure 10c display a wall-climbing effect towards lower frequency energy, but evidence of longshore flow pulsing is apparent on 21/4/94, occurring across a wide frequency band of approximately 0.025–0.007 Hz (40–143 s). Pulses appear to be of longer duration than in the rip-neck, but exhibit a similar fluctuation range in flow velocity (Figure 10b). In contrast, the spectra for 18/4/94 is dominated by red-shifting with no distinct energy peak. There are no significant spectral peaks at swell and wind-wave frequencies in either spectra shown in Figure 10c.

As shown in Figure 11, the relative amounts of energy variance from current spectra associated with wind (*%wind*), swell (*%swell*), and infragravity (*%inf*) frequency bands varied both over time and between components of the rip system during PB1. In the rip-neck, *%wind* clearly dominated over *%swell* and *%inf* with 53% of the spectral energy compared to 35% and 9% respectively on 18/4/94 (Figure 11a). This is not surprising, since storm waves were still subsiding at this time. By 23/4/94 however, with an absence of storm waves and the beach characterised by TBR morphology (Figure 2f), spectral energy was equally dominated by *%inf, %swell,* and *%wind* with each contributing $\cong$ 30% of the kinetic energy of rip flow (Figure 11a). Overall, *%inf* increased gradually from 8–32% as *%wind* decreased from 60–32%, while *%swell* remained relatively constant throughout the experiment. In contrast, flow in the northern feeder was clearly dominated by energy at infragravity frequencies with *%inf* being approximately twice as great as *%swell* and *%wind* combined (Figure 11b). As the feeder channel began to infill and narrow between 18/4 and 21/4/94, *%inf* increased from 42% to 68% (Figure 11b). It should be noted, however, that although the relative component of variance attributed to infragravity wave frequencies in the feeder was higher than in the rip-neck, the actual magnitude of infragravity energy was higher in the rip-neck (Figure 9c).

FLOW DISCHARGE

It is often assumed that most, if not all, of the water flowing in the rip-neck is delivered via the feeders. Therefore feeder discharge should approximate rip-neck discharge. To examine this idea, estimates of both offshore rip discharge and onshore discharge through mass transport by the waves must be obtained. A gross assumption can be made that rip currents return all of the water transported onshore, thereby maintaining an overall mass balance of water in the nearshore circulation cell. Mean discharge through the rip-neck ($\bar{Q}_{rip}$) can be approximated by

$$\bar{Q}_{rip} = \bar{u}_r \bar{A}_r \quad (2)$$

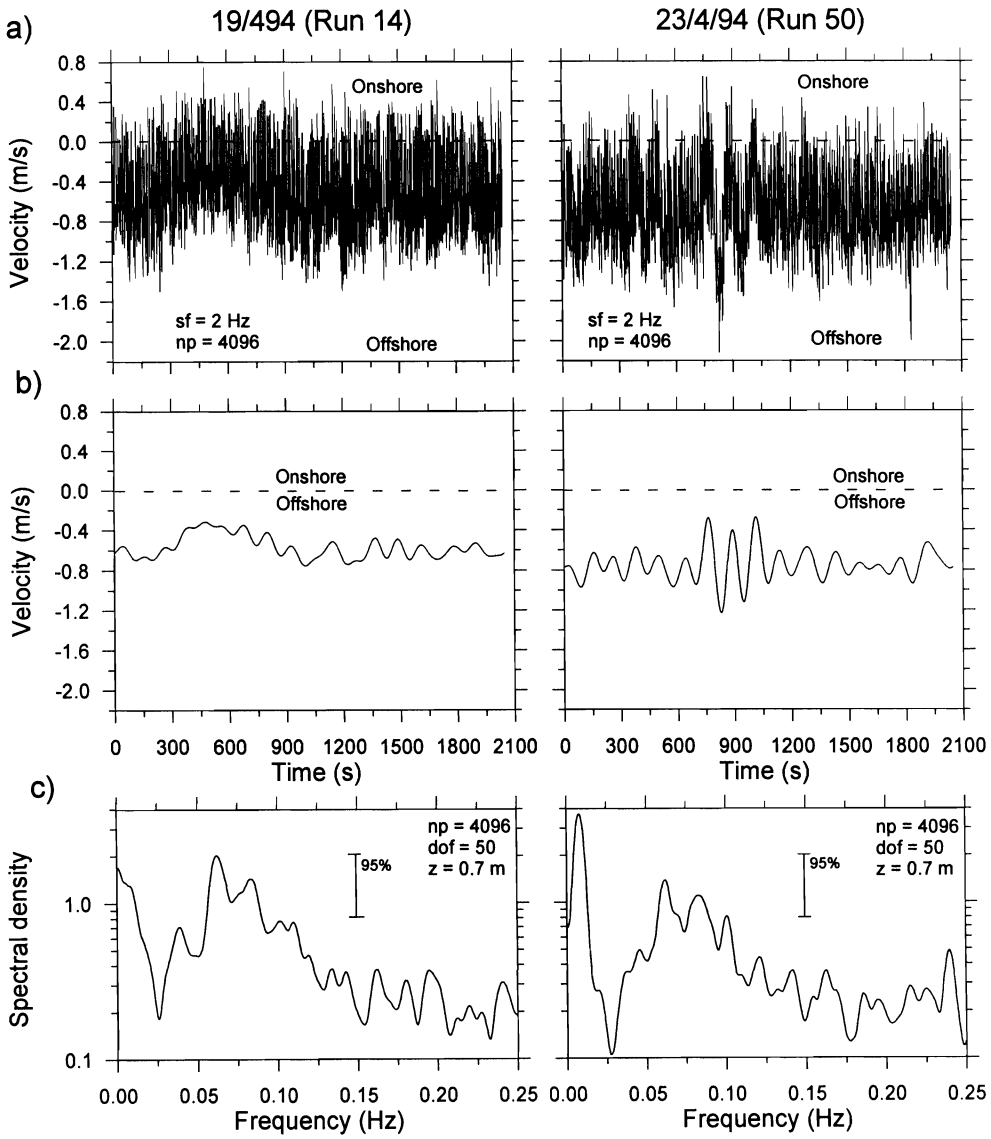

Figure 9. Flow velocity characteristics of the rip-neck on 19/4/94 (Run 14) and 23/4/94 (Run 50) as illustrated by: a) raw time series of u_r; b) low-pass filtered time series (cut-off = 0.01 Hz); and c) current energy spectra (variance spectral density in $m^2\Delta f^{-1}$). Note: z = sensor elevation, sf = sampling frequency, np = number of points, and dof = degrees of freedom.

where $\bar{A}_r$ is the mean rip-neck cross-sectional area and contains both the area within the channel banks and the area of water column between the banks extending upwards to the water level. Following the model outlined in AAGAARD *et al.* (1997), the onshore discharge (Q_{on}) was calculated using the approach of SVENDSEN (1984) who showed that the amount of water carried onshore by breaking waves is associated with mass transport in the waves by Stokes drift (Q_d) and the wave roller (Q_r), such that:

$$Q_{on} = (Q_d + Q_r)\lambda_r \quad (3)$$

where λ_r is the longshore distance of the rip cell system. Full derivations of Q_d and Q_r are given by AAGAARD *et al.* (1997).

Figure 12 shows the relationship between measured rip-neck discharges from Eq. (2) and predicted onshore discharges from Eq. (3). $\bar{Q}_{rip}$ is representative of average daily conditions at the location of the rip-neck pod and values of A_r were determined from the contour plots in Figures 2 and 3. Values of λ_r were estimated from surveys and oblique photographs. For PB1, λ_r decreased from 400 m on 18/4/94 to 100 m on 24/4/94. A value of 60 m was representative of the rips observed during PB2. Overall, the relationship between predicted onshore and measured offshore discharges (Figure 12) is reasonable (R^2 = 0.81) and suggests that the onshore mass transport is returned seaward by the rip current. If anything, the distribution of scatter suggests that measured discharge is larger than predicted discharge.

It does not appear, however, that all of the onshore dis-

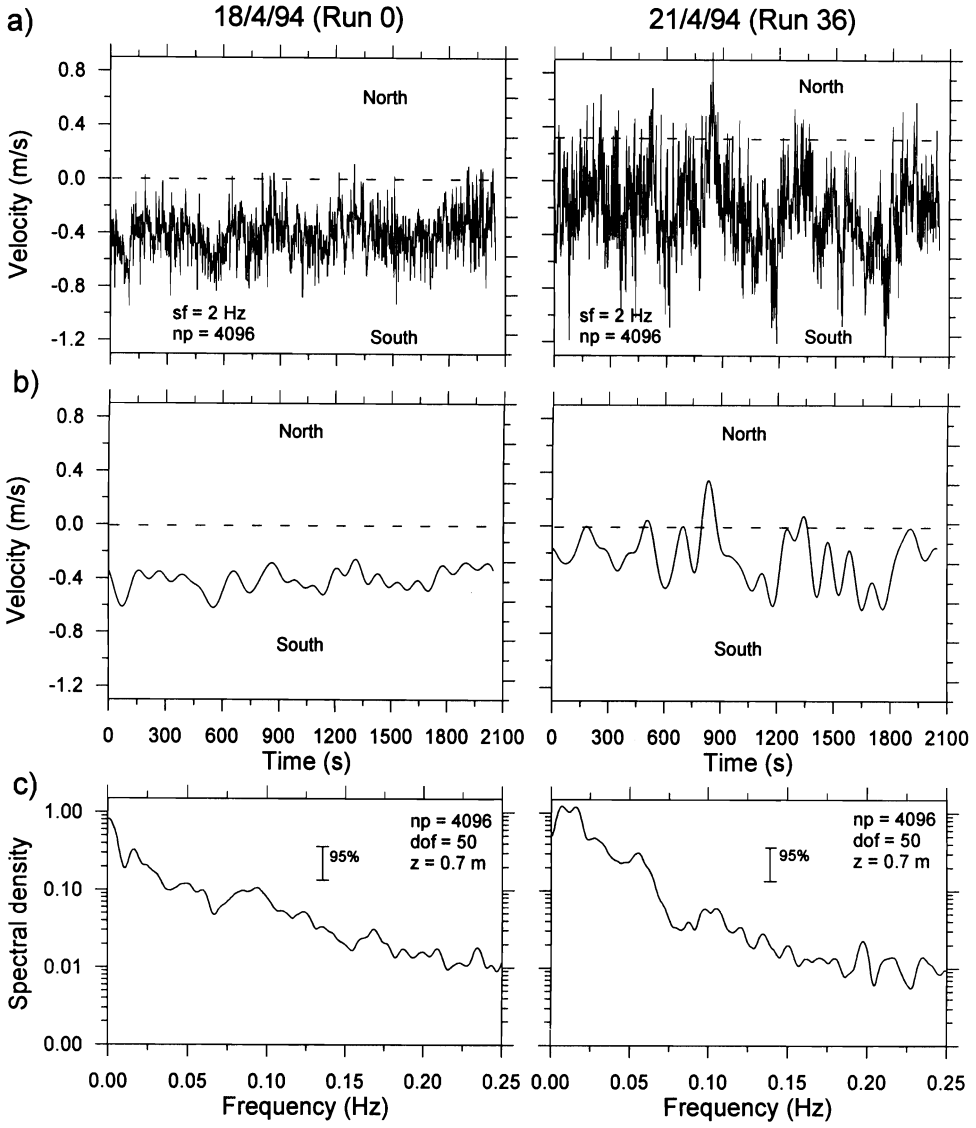

Figure 10. Flow velocity characteristics of the northern feeder on 18/4/94 (Run 0) and 21/4/94 (Run 36) as illustrated by: a) raw time series of u; b) low-pass filtered time series (cut-off = 0.01 Hz); and c) current energy spectra (variance spectral density in $m^2\Delta f^{-1}$). Note: z = sensor elevation, sf = sampling frequency, np = number of points, and dof = degrees of freedom.

charge is delivered to the rip-neck via the rip feeders. Table 2 lists daily percentage contributions of rip-neck discharge determined from instrument pods deployed in the north and south feeders, and at the base of the rip-neck (Figure 2). Discharges in the northern feeder were always less than 10% and decreased over time as the feeder infilled. The exception to this was 22/4/94, when the feeder pod was located close to the base of the rip (Figure 2e). The southern feeder initially contributed approximately 30% of rip-neck discharge, indicating flow dominance over the northern feeder, but similarly decreased in discharge over time as the system continued to evolve. The combined feeder discharges were always significantly less than rip-neck discharge (Table 2). Discharges recorded at the base of the rip-neck initially accounted for approximately 50% of rip-neck discharge, but similarly decreased over time.

DISCUSSION

The purpose of this study was to describe and quantify the kinematic behaviour of rip current systems with a secondary aim being to examine the potential influence of direct topographical control on rip flow. The temporal characteristics of rip system flow recorded in this study support the observations made by WRIGHT and SHORT (1984) that rip velocities may increase after the longshore bar and trough state (LBT)

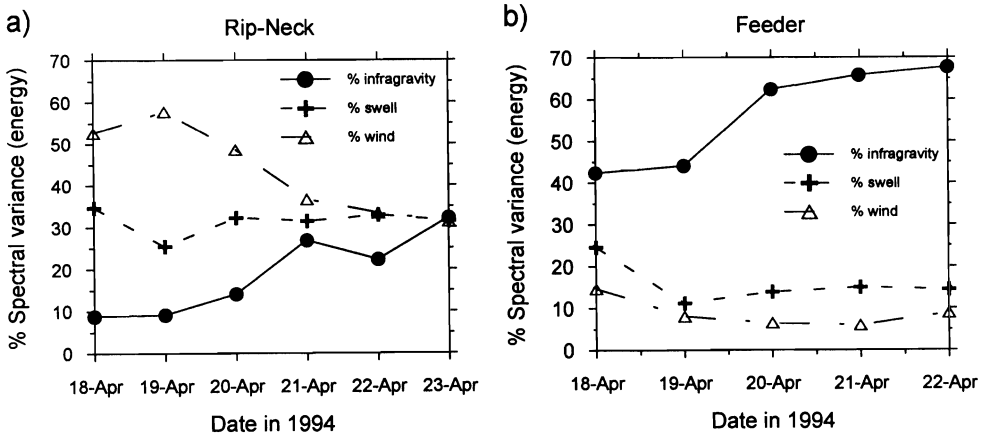

Figure 11. The temporal variation of *%wind, %swell,* and *%inf* (see Methods for definitions) of the total energy in the current spectra during PB1 in: a) the rip-neck; and b) the feeders (only 22/4/94 is representative of the southern feeder).

and peak in the transverse bar and rip state (TBR). Similarly, their suggestion that strong rip flow on the order of 1 m s^{-1} may persist on TBR beaches when waves are reasonably low (H_b<1 m) is also quantified. SHORT (1985) attributed this pattern of increasing flow velocity during decreasing energy levels to a progressive confinement of flow to smaller, narrower channels, but was unable to support this idea with field measurements. A detailed examination of topographic data from the PB1 experiment by BRANDER (1999) however, found a strong inverse relationship between cross-sectional rip-neck channel area and rip-neck velocity.

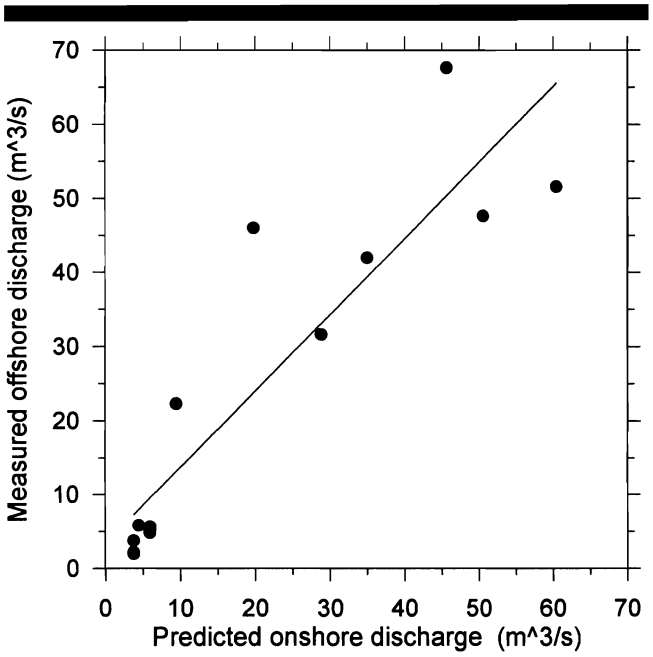

Figure 12. Relationship between predicted onshore discharge (Eq. 3) and measured offshore discharge (Eq. 2) at the rip-neck for each day of PB1 and PB2.

It would be expected that topographic confinement of rip flow would be enhanced at low tide rather than at high tide and the present study supports the findings of other studies (SHEPARD *et al.,* 1941; SHEPARD and INMAN, 1950; INMAN and QUINN, 1952; MACKENZIE, 1958; SONU, 1972; SHORT and HOGAN, 1994; AAGAARD *et al.,* 1997) that rip flow velocities are generally stronger towards low tide. SONU (1972) stated emphatically that wave breaking over inner bars was essential to the formation of rip circulation and that the intensity of breaking, controlled by the tide, corresponded with a proportionally stronger circulation. This important point raises the debate as to whether morphologic control is manifest by distinct flow channelisation or by the enhancement of set-up gradients generated by wave dissipation over varying morphologic beach states. Without measurements of set-up, it is difficult to reconcile this problem.

The results from this study do, however, provide some support for the idea of morphologic flow constriction. The major difference between the response of rip-neck and feeder channel flow to tidal level during PB1 was that the former maintained a relatively strong offshore flow throughout the tidal cycle whereas flow towards the rip-neck in the northern feeder approached 0 m s^{-1} and sometimes reversed around high tide (Figure 5c). This cessation of current flow was not restricted to the northern feeder since all three rips during the PB2 experiment experienced the same phenomenon (Figure 5d). The commonality between the northern feeder channel

Table 2. *Relative contributions of measured feeder and base of rip-neck discharges to overall rip-neck discharge ($\bar{Q}_{rip}$). Instrument pod locations are given on Figure 2. "—" indicates no data.*

Day	% N. Feeder	% S. Feeder	% Both Feeders	% Base Rip-neck
18/4/94	8.3	—	—	54
19/4/94	6.9	31.6	38.5	61
20/4/94	6.3	—	—	45
21/4/94	2.4	—	—	26
22/4/94	6.7	8.6	16.3	—

and the rip channels of PB2 is that both were characterised by narrower widths and more pronounced channel banks than the rip-neck channels observed during PB1 (Figures 2 and 3). The implication here is that increasingly smaller and constricted channels are more sensitive to tidally-induced water depth changes. An interesting hypothesis is that these patterns are related to the concept of underfit and overfit rip channels postulated by SHORT (1985), whereby the velocity of flow at low tide in a deeply incised channel will remain relatively constant with rising water level because the area available for flow is constrained by the morphologic banks and will not vary greatly with changing water depth within the channel. However, when water level overtops the banks the velocity of flow will decrease since the area available for flow expands rapidly.

In terms of spatial characteristics of rip flow kinematics, early theoretical work by TAM (1973) proposed that rip current velocity decreases in the direction of flow. Subsequently, SONU (1972) and SASAKI and HORIKAWA (1975) suggested that velocity in the rip current remains relatively constant offshore. However, results from this study clearly indicate that the dominant spatial pattern of rip current flow is a seaward increase in velocity (Figure 7a,b). This result is consistent with the observations of SHEPARD and INMAN (1950) and BOWMAN *et al.* (1988b), who found that mean velocity increased from the longshore feeder to rip-neck.

This study provides quantitative evidence that flow velocity increases away from the channel bank and is maximised towards the deepest part of the rip-neck channel (Figure 7c). Since all three instrument pods were deployed at approximately the same distance offshore, it is unlikely that this variation in cross-rip velocity is driven by external forcing variables and is determined more by channel geometry and frictional resistance. This supports the surface measurements of SASAKI and HORIKAWA (1975) that maximum velocities in the rip-neck occurred towards the middle and, since the current flowed along bottom contours, topography must exert a strong influence on the currents.

Vertical velocity profiles of flow in both the rip-neck and feeder channels show an increase in velocity away from the bed followed by a decrease towards the surface (Figure 8). These results are in contrast to WRIGHT *et al.* (1986) who suggested that maximum seaward flow in the rip occurred at the surface, but are in partial agreement with those of SONU (1972) who found that flow velocity increased upwards in rip flow and that the locus of peak velocity in the profiles shifted upward with distance seaward in the rip. The latter is hard to assess in this study since only one vertical array was deployed each day. There is however, a logical explanation behind the shape of the profiles in Figure 8. The initial upward increase in velocity from the lowest to middle sensor can be attributed to reduced frictional affects due to bed roughness whereas the subsequent upward decrease in velocity towards the surface can be attributed to the greater effect of onshore orbital velocities from wave motions in the rip channel.

Significant amounts of infragravity energy were found in both the rip-neck and feeder channels (Figure 11). This is in direct contrast with the results of BOWMAN *et al.* (1988a; b; 1992) who found little infragravity energy present in their rip feeder and rip-neck environments. Evidence of rip flow pulsing at infragravity frequencies was identified in Figures 9 and 10. The idea that rips exhibit pulses in the strength of their velocity was first suggested by SHEPARD and INMAN (1950) and MCKENZIE (1958). SONU (1972) also noted that rip circulation pulsed at surf beat frequencies and that this effect was enhanced at low tide. Although never measured, it is commonly suggested (*e.g.* SHORT, 1985; AAGAARD and MASSELINK, 1999) that rip pulsing is related to energy at infragravity frequencies and may be related to wave groupiness. TANG and DALRYMPLE (1988) discussed the theoretical interactions between incident wave groups and rip currents, but their results were inconclusive.

Rip pulsing measured during this study occurs at periods of several minutes. These low frequency motions therefore fall within the range corresponding to far-infragravity waves, or shear waves (BOWEN and HOLMAN, 1989; OLTMAN-SHAY *et al.,* 1989; AAGAARD and MASSELINK, 1999), which are manifest by shear instabilities in the longshore current. FOWLER and DALRYMPLE (1990) used theory and laboratory studies to suggest that forcing by wave groups can result in migrating rip currents which display a low frequency motion in the far-infragravity band. The implication in this study is that shear instability may also be present in rip current flow, both in the presence and absence of longshore feeders. It is interesting to note that infragravity energy was dominant in the feeder channel and in the rip-neck during the TBR state, both of which are characterised by pronounced channel topography. However, due to a lack of pressure sensors deployed over the bars, and the malfunction of some of the pressure sensors at critical times, it is not possible to adequately assess whether these oscillations are driven by wave groups or by trapped resonance within the surf zone.

Results pertaining to offshore discharge via the rip system (Table 2) suggest two important patterns of rip feeder behaviour. First, feeder channel flow does not account for all of the water entering the rip irrespective of the stage of morphodynamic rip evolution. Second, as the feeder channels become progressively infilled, their contribution to rip-neck discharge tends to decrease. These findings suggest that a major proportion of water discharging through the rip-neck must enter the rip from other sources. In the case of intermediate beaches, such as those in this study, a major source is likely to be water entering, or draining, sideways into the rip-neck from the adjacent nearshore bars. As planimetric morphologic area of these bars increases during an accretionary beach cycle (Figure 2), this source area would potentially become more important over time. This phenomenon of water streaming sideways into the rip-neck was observed directly in the field and appeared to peak under TBR and LTT beach states, when planimetric bar area is maximised, particularly around low tide. The implication here is that the traditional idea of longshore feeders delivering most of the water into the rip-neck on intermediate beaches may not be entirely valid.

CONCLUSION

As outlined in the preceding discussion, this study has provided both new quantitative information on the tem-

poral and spatial characteristics of rip flow kinematics and additional quantitative support to findings of previous studies. Most significantly, direct evidence of rip pulsing at infragravity frequencies is presented and is considered to be a process of major importance to rip flow. The results of this study also suggest that the traditional understanding of the pathways through which water enters rip channels on intermediate beaches needs further attention. The argument has been made in this study that many aspects of rip flow can be attributed directly to the role of topographic forcing and morphologic control. It can be debated however, that these findings are merely a response of the overall adjustment of wave dissipation and set-up gradients in response to changing morphologic patterns. Further research is clearly necessary in order to assess the complex morphodynamic feedback relationships which exist between the set-up gradients driving rip flow and the subsequent modification of flow through topographic control. Until this problem is adequately addressed, it is suggested that further understanding of rip current behaviour will be limited.

ACKNOWLEDGEMENTS

This research was supported by funds made available by the School of Geosciences (Geography), University of Sydney. The authors are indebted to the prime field crew of Michael Hughes, Gui Lessa, Gerd Masselink, Justin Meleo, Dave Mitchell, Matt Potter, Anne Sorber and Ian Turner. Without their efforts, the experiments would not have been possible. Thanks are also due to the Palm Beach Surf Life Saving Club for their hospitality and to John Roberts (Cartographer, Univ. of Sydney) for preparation of Figure 1. We are also very appreciative of the constructive comments and input made by Brian Greenwood and Troels Aagaard on an earlier version of the manuscript.

LITERATURE CITED

AAGAARD, T. and GREENWOOD, B., 1995. Longshore and cross-shore suspended sediment transport at far infragravity frequencies in a barred environment. *Continental Shelf Research,* 15 (10), 1235–1249.

AAGAARD, T. and MASSELINK, G., 1999. The Surf Zone. *In: Handbook of Beach and Shoreface Morphodynamics* SHORT, A.D. (ed.), John Wiley & Sons, p. 72–118.

AAGAARD, T.; GREENWOOD, B., and NIELSEN, J., 1997. Mean currents and sediment transport in a rip channel. *Marine Geology,* 140 (1/2), 25–45.

BASCO, D.R., 1983. Surfzone currents. *Coastal Engineering,* 7, 331–355.

BOWEN, A.J. and HOLMAN, R.A., 1989. Shear instabilities of the mean longshore current. 1. Theory. *Journal of Geophysical Research,* 94, 18023–18030.

BOWMAN, D.; ARAD, D.; ROSEN, D.S.; KIT, E.; GOLDBERY, R., and SLAVICZ, A., 1988a. Flow characteristics along the rip current system under low-energy conditions. *Marine Geology,* 82, 149–167.

BOWMAN, D.; ROSEN, D.S.; KIT, E.; ARAD, D., and SLAVICZ, A., 1988b. Flow characteristics at the rip current neck under low energy conditions. *Marine Geology,* 79, 41–54.

BOWMAN, D.; BIRKENFIELD, H., and ROSEN, D.S., 1992. The longshore flow component in low-energy rip channels: the Mediterranean, Israel. *Marine Geology,* 108, 259–274.

BRANDER, R.W., 1999. Field observations on the morphodynamic evolution of a low-energy rip current system. *Marine Geology,* 157, 199–217.

FOWLER, R.E. and DALRYMPLE, R.A., 1990. Wave group forced nearshore circulation. *Proceedings of the 22st International Conference on Coastal Engineering,* ASCE, 729–742

FOX, W.T. and DAVIS, R.A., JR., 1974. *Beach processes on the Oregon Coast, July, 1973.* Office of Naval Research, Williams College, Technical Report 12, 85 p.

HEGGE, B.J. and MASSELINK, G., 1996. Spectral analysis of geomorphic time series: auto-spectrum. *Earth Surface Processes and Landforms,* 21, 1021–1040.

HUNTLEY, D.A.; HENDRY, M.D.; HAINES, J., and GREENIDGE, B., 1988. Waves and rip currents on a Caribbean pocket beach, Jamaica. *Journal of Coastal Research,* 4(1), 69–79.

INMAN, D.L. and QUINN, W.H., 1952. Currents in the surf zone. *Proceedings of the 2nd International Conference on Coastal Engineering,* ASCE, 24–36.

KOMAR, P.D., 1998. *Beach Processes and Sedimentation.* Prentice Hall, 544 p.

MCKENZIE, P., 1958. Rip-current systems. *Journal of Geology,* 66, 103–113.

NIELSEN, P., 1988. Analysis of natural waves by local approximations. *Journal of Waterway, Port, Coastal, and Ocean Engineering,* 115, 384–396.

NEILSEN, P., 1992. *Coastal Bottom Boundary Layers and Sediment Transport.* World Scientific, London, 324 p.

NIELSEN, P. and COWELL, P.J., 1981. *Calibration and data correction procedures for flow meters and pressure transducers commonly used by the Coastal Studies Unit.* Coastal Studies Unit, University of Sydney Tech. Rep. 81/1.

N.S.W. Public Works Manly Hydraulics Laboratory, 1994. Wave and tide data for Long Reef and Sydney stations.

OLTMAN-SHAY, J.; HOWD, P.A., and BIRKMEIER, W.A., 1989. Shear instabilities of the mean longshore current. 2. Field observations. *Journal of Geophysical Research,* 94, 18031–18042.

SASAKI, T. and HORIKAWA, T., 1975. Nearshore current system on a gently sloping bottom. *Coastal Engineering in Japan,* 18, 123–142.

SHEPARD, F.P.; EMERY, K.O., and LAFOND, E.C., 1941. Rip currents: a process of geological importance. *Journal of Geology,* 49, 337–369.

SHEPARD, F.P. and INMAN, D.L., 1950. Nearshore circulation related to bottom topography and wave refraction. *Transactions of the American Geophysical Union,* 31(4), 555–565.

SHORT, A.D., 1985. Rip current type, spacing and persistence, Narrabeen beach, Australia. *Marine Geology,* 65, 47–71.

SHORT, A.D. and HOGAN, C.L., 1994. Rip currents and beach hazards: their impact on public safety and implications for coastal management. *Journal of Coastal Research,* Special Issue No. 12, 197–209.

SHORT, A.D. and TRENAMAN, N.L., 1992. Wave climate of the Sydney region, an energetic and highly variable ocean wave regime. *Australian Journal of Marine and Freshwater Research,* 43, 765–791.

SMITH, J.A. and LARGIER, J.L., 1995. Observations of nearshore circulation: rip currents. *Journal of Geophysical Research,* 100(C6), 10967–10975.

SONU, C.J., 1972. Field observation on nearshore circulation and meandering currents. *Journal of Geophysical Research,* 77, 3232–3247.

SVENDSEN, I.A., 1984. Mass flux and undertow in the surf zone. *Coastal Engineering,* 8, 347–365.

TALBOT, M.M.B. and BATE, G.C., 1987a. Distribution patterns of rip frequency and intensity in Algoa Bay, South Africa. *Marine Geology,* 76, 319–324.

TALBOT, M.M.B. and BATE, G.C., 1987b. Rip current characteristics and their role in the exchange of water and surf diatoms between the surf zone and nearshore. *Estuarine, Coastal and Shelf Science,* 25, 707–720.

TAM, C.K.W., 1973. Dynamics of rip currents. *Journal of Geophysical Research,* 78(12), 1937–1943.

TANG, E.C.S. and DALRYMPLE, R.A., 1988. Nearshore circulation: b. rip currents and wave groups. *In: Nearshore Sediment Transport* SEYMOUR, R.J. (ed.). Plenum, p. 205–230.

WRIGHT, L.D.; CHAPPELL, J.; THOM, B.G.; BRADSHAW, M.P., and COWELL, P., 1979. Morphodynamics of reflective and dissipative beach and inshore systems: Southeastern Australia. *Marine Geology,* 32, 105–140.

WRIGHT, L.D.; COFFEY, F.C., and COWELL, P.J., 1980. *Nearshore Oceanography and Morphodynamics of the Broken Bay-Palm Beach Region, N.S.W.: Implications for Offshore Dredging.* Coastal Studies Unit, University of Sydney, Technical Report No. 80/1, 208 p.

WRIGHT, L.D.; NIELSEN, P.; SHI, N.C., and LIST, J.H., 1986. Morphodynamics of a bar-trough surf zone. *Marine Geology,* 50, 97–128.

WRIGHT, L.D. and SHORT, A.D., 1984. Morphodynamic variability of surf zones and beaches: a synthesis. *Marine Geology,* 56, 93–118.